Biophysical Journal Volume 71 October 1996 2192–2200

Dielectric Behavior of Wild-Type Yeast and Vacuole-Deficient Mutant Over a Frequency Range of 10 kHz to 10 GHz

Koji Asami* and Takeshi Yonezawa#

*Institute for Chemical Research, Kyoto University, Uji, Kyoto 611 and #Production Division I, Suntory Ltd., Oyamazaki, Shimamoto-cho, Mishima-gun, Osaka 618, Japan

ABSTRACT Dielectric behavior of *Saccharomyces cerevisiae* wild-type and vacuole-deficient mutant cells has been studied over a frequency range of 10 kHz to 10 GHz. Both types of cells harvested at the early stationary growth phase showed dielectric dispersion that was phenomenologically formulated by a sum of three separate dispersion terms: β_1-dispersion (main dispersion) and β_2-dispersion (additional dispersion) and γ-dispersion due to orientation of water molecules. The β_1-dispersion centered at a few MHz, which has been extensively studied so far, is due to interfacial polarization (or the Maxwell-Wagner effect) related to the plasma membrane. The β_2-dispersion for the vacuole-deficient mutant centered at ~50 MHz was explained by taking the cell wall into account, whereas, for the wild-type cells, the β_2-dispersion around a few tens MHz involved the contributions from the vacuole and cell wall.

INTRODUCTION

Biological cells show dielectric dispersion (termed β_1-dispersion) due to interfacial polarization (or the Maxwell-Wagner effect) related to the plasma membrane (Schwan, 1957; Cole, 1968; Foster and Schwan, 1989) and additional dispersions (termed β_2-dispersion) at the higher frequency side of the β_1-dispersion (Schwan, 1987). In our previous studies (Asami et al., 1989; Asami and Yamaguchi, 1992) we demonstrated that the β_2-dispersions observed for lymphocytes and plant protoplasts are attributed to the interfacial polarization related to intracellular organelles such as the nucleus, vacuole, and chloroplasts. The dielectric dispersions were not interpreted in terms of the "single-shell" model but were successfully simulated by the "double-shell" model (Irimajiri et al., 1978) and its modified model, in which intracellular organelles were considered. The "double-shell" or "three-shell" model (Furhr et al., 1985) also interpreted the broadening of dielectrophoretic and electrorotational spectra of plant protoplasts (Gimsa et al., 1985) and neurospora slime and murine myeloma cells (Gimsa et al., 1991).

Yeast cells usually have vacuoles that occupy 10 to 50% of their cell volume, thereby being expected to show β_2-dispersion. In addition, the cell wall whose electrical properties differ from those of the external medium is supposed to give rise to another dispersion. However, most of the studies on dielectric behavior of yeast cells (Sugiura et al., 1964; Sugiura and Koga, 1965; Asami et al., 1976, 1977; Asami, 1977a,b; Harris and Kell, 1983) have been confined to the β_1-dispersion centered at ~1 MHz. Their dielectric behavior above 10 MHz has not been investigated in detail so far because of technical difficulties encountered in high-frequency measurements.

In this study we extend the previous dielectric measurements of yeast cells to a high frequency range up to 10 GHz in an attempt to detect the β_2-dispersion, if any. Comparison in dielectric behavior is made between wild-type and its vacuole-deficient mutant cells to clarify the contribution of the vacuole to the β_2-dispersion.

THEORY

Electrical models of wild-type yeast and vacuole-deficient mutant

Dielectric behavior of simple cells that lack intracellular organelles and possess a plasma membrane is well simulated by a simple electrical model, the so called "single-shell" model (model A in Fig. 1) (Pauly and Schwan, 1959; Hanai et al., 1979). However, yeast cells are surrounded by a cell wall and include internal organelles, such as the vacuole, nucleus, and mitochondria, its model being more complicated. As electrical models for yeast cells, therefore, we propose models B and C (Fig. 1). In model B, we add one shell (that corresponds to the cell wall) exterior to the shell-sphere (model A). In model C, a shell-sphere (or a vesicle) that corresponds to the vacuole is incorporated into the spherical core of model B. We take into account only the vacuole that occupies a large part of the cytoplasm. The contribution of the other organelles might be relatively small compared with that of the vacuole, because the nucleus with the leaky nuclear membrane is weakly polarized in an electric field and the volume concentration of mitochondria and other small organelles are negligibly small. Models B and C are a special case of the "multi-shell" model (Irimajiri et al., 1979).

In the following subsections, we will derive dielectric formulas for models B and C, which are conveniently expressed using complex permittivity that is defined as $\epsilon^* =$

Received for publication 18 March 1996 and in final form 27 June 1996.

Address reprint requests to Dr. K. Asami, Institute for Chemical Research, Kyoto University, Uji, Kyoto 611, Japan. Tel.: +81-774-32-3111; Fax: +81-774-33-1154; E-mail: asami@tampopo.kuicr.kyoto-u.ac.jp.

0006-3495/96/10/2192/09 $2.00

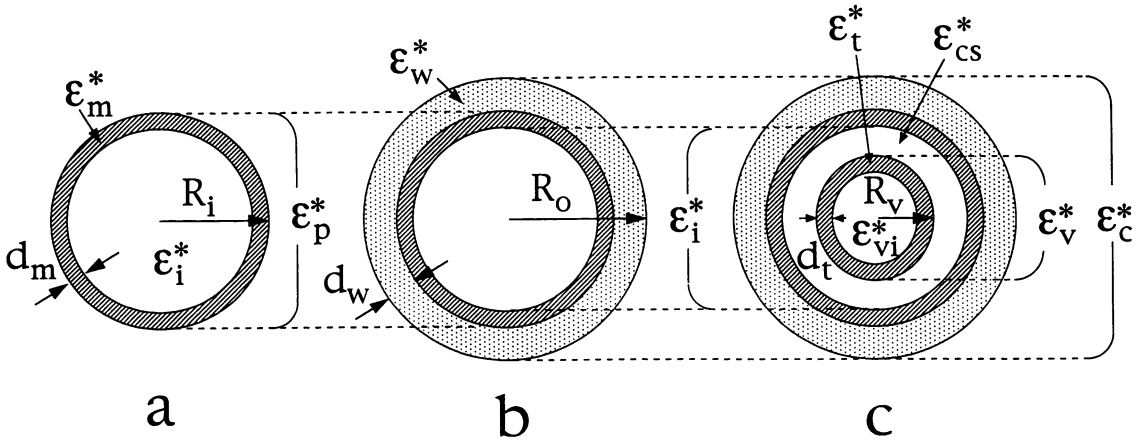

FIGURE 1 Electrical models for yeast cells. (*a*) Model A that is a sphere covered with a shell: ϵ^* is complex relative permittivity defined as $\epsilon^* = \epsilon - j\kappa/\omega\epsilon_0$, where ϵ is relative permittivity, κ conductivity, $\omega = 2\pi f$, f frequency, ϵ_0 the permittivity of vacuum and $j^2 = -1$. The subscripts m, i, and p of ϵ^* refer to the shell (plasma membrane in this case), the inner phase (cytoplasm) and the entire shell-sphere (protoplasm), respectively. R_i is the radius of the shell-sphere and d_m is the shell thickness. (*b*) Model B that is a sphere covered with two adjoining shells. The subscript w of ϵ^* refers to the outer shell (cell wall). R_o is the outer radius and d_w is the outer shell thickness. (*c*) Model C that is a sphere, including a vesicle, covered with two adjoining shells. The subscripts cs, t, vi, v, and c of ϵ^* refer to the intershell space, the shell (tonoplast) of the vesicle, the inner phase of the vesicle, the whole vesicle (vacuole), and the whole cell, respectively. R_v is the radius of the vesicle and d_t is the thickness of the vesicle shell.

$\epsilon - j\kappa/\omega\epsilon_0$, where ϵ is relative permittivity, κ conductivity, ϵ_0 the permittivity of vacuum, $\omega = 2\pi f$, f frequency, and $j = (-1)^{1/2}$.

Equivalent complex permittivity for model B

The equivalent complex permittivity ϵ_c^* of model B in which a shell-sphere (of equivalent complex permittivity ϵ_p^*) is covered with a shell (of complex permittivity ϵ_w^*) is expressed as (Maxwell, 1873; Wagner, 1914):

$$\epsilon_c^* = \epsilon_w^* \frac{2(1 - v_2)\epsilon_w^* + (1 + 2v_2)\epsilon_p^*}{(2 + v_2)\epsilon_w^* + (1 - v_2)\epsilon_p^*} \quad (1)$$

where $v_2 = (1 - d_w/R_o)^3$, R_o is the outer radius of the sphere and d_w is the outer shell thickness.

The equivalent complex permittivity ϵ_p^* of the inner shell-sphere that is a homogeneous sphere (of complex permittivity ϵ_i^*) covered with a shell (of ϵ_m^*) is given by

$$\epsilon_p^* = \epsilon_m^* \frac{2(1 - v_1)\epsilon_m^* + (1 + 2v_1)\epsilon_i^*}{(2 + v_1)\epsilon_m^* + (1 - v_1)\epsilon_i^*} \quad (2)$$

where $v_1 = (1 - d_m/R_i)^3$, R_i is the radius of the inner shell-sphere and d_m is the inner shell thickness.

Equivalent complex permittivity for model C

To obtain the equivalent complex permittivity ϵ_c^* of model C, the core of ϵ_i^* in model B is replaced by a vesicle (of equivalent complex permittivity ϵ_v^*) surrounded with an intershell space (of complex permittivity ϵ_{cs}^*). Thus, ϵ_i^* is written as:

$$\epsilon_i^* = \epsilon_{cs}^* \frac{2(1 - v_3)\epsilon_{cs}^* + (1 + 2v_3)\epsilon_v^*}{(2 + v_3)\epsilon_{cs}^* + (1 - v_2)\epsilon_v^*} \quad (3)$$

where $v_3 = (R_v/(R_i - d_m))^3$ and R_v is the radius of the vesicle. The complex permittivity ϵ_v^* of the vesicle that is composed of a core of ϵ_{vi}^* and a shell of ϵ_t^* is given by

$$\epsilon_v^* = \epsilon_t^* \frac{2(1 - v_4)\epsilon_t^* + (1 + 2v_4)\epsilon_{vi}^*}{(2 + v_4)\epsilon_t^* + (1 - v_4)\epsilon_{vi}^*} \quad (4)$$

where $v_4 = (1 - d_t/R_v)^3$ and d_t is the shell thickness of the vesicle. The ϵ_c^* for model C is, thus, calculated from Eqs. 1–4.

Complex permittivity of cell suspension

In our previous dielectric studies on yeast cells we used Pauly-Schwan's equation (Pauly and Schwan, 1959) that is based on Wagner's mixture equation (Wagner, 1914), which holds for only dilute spherical particle suspensions (volume fraction $p < 0.1$) in principle. Because in this study dielectric measurements were carried out with concentrated cell suspensions to ensure the accuracy and to eliminate the influence of cell sedimentation, we adopted Hanai's mixture equation (Hanai, 1960; 1968) instead of Wagner's equation, although Davey et al. (1992) claimed that Pauly-Schwan's equation is also applicable to cell suspensions at high volume fractions. Hanai's equation that is the extension of Bruggeman's equation (Bruggeman, 1935) to complex permittivity has been confirmed to give better simulations than Wagner's equation for various concentrated colloidal sus-

pensions including biological cell suspensions at volume fractions up to 0.7 (Irimajiri et al., 1975; Ishikawa et al., 1981; Hanai et al., 1982; Clausse, 1983; Zhang et al., 1983; Kaneko et al., 1991).

According to Hanai's theory (Hanai, 1960), the complex permittivity ϵ^* of a system in which spherical cells (of equivalent complex permittivity ϵ_c^*) are suspended in a continuous phase (of complex permittivity ϵ_a^*) at volume fraction P is given by

$$\frac{\epsilon^* - \epsilon_c^*}{\epsilon_a^* - \epsilon_c^*}\left(\frac{\epsilon_a^*}{\epsilon^*}\right)^{1/3} = 1 - P \tag{5}$$

Approximate equations at low frequencies

It is helpful to present approximate equations of Eq. 5 at low frequencies, from which the membrane capacitance and the conductivity of the cell wall can be estimated. Because the plasma membrane is extremely thin compared with the cell radius ($d_m/R_i \ll 1$, and thus $v_1 \approx 1 - 3\,d_m/R_i$) and its conductivity is negligibly small compared with the internal conductivity ($\kappa_m \ll \kappa_i$), the low-frequency limits of the equivalent relative permittivity ϵ_{pl} and conductivity κ_{pl} of the inner shell-sphere in model B are obtained from Eq. 2.

$$\epsilon_{pl} = \epsilon_m \frac{1 + 2v_1}{1 - v_1} \approx \epsilon_m R_i/d_m = C_m R_i/\epsilon_0 \tag{6}$$

$$\kappa_{pl} = \kappa_m \frac{1 + 2v_1}{1 - v_1} \approx \kappa_m R_i/d_m \approx 0 \tag{7}$$

where C_m is the membrane capacitance (given by $C_m = \epsilon_m\epsilon_0/d_m$). These equations are also applicable to model C, irrespective of the presence of the intracellular structure. Because $\kappa_{pl} \ll \kappa_w$ and $\epsilon_{pl} \gg \epsilon_w$, Eq. 1 provides the equivalent relative permittivity ϵ_{cl} and conductivity κ_{cl} of the cell at low frequencies as:

$$\epsilon_{cl} = \epsilon_w \frac{2(1 - v_2)}{2 + v_2} + 9\epsilon_{pl}\frac{v_2}{(2 + v_2)^2} \approx 9\epsilon_{pl}\frac{v_2}{(2 + v_2)^2} \tag{8}$$

$$\kappa_{cl} = \kappa_w \frac{2(1 - v_2)}{2 + v_2} \tag{9}$$

The low-frequency limits of the equivalent relative permittivity ϵ_l and conductivity κ_l for the suspension of the cells with ϵ_{cl} and κ_{cl} are derived from Eq. 5 by Hanai (1968).

$$\epsilon_l = 3\left(\frac{\epsilon_a - \epsilon_{cl}}{\kappa_a - \kappa_{cl}} + \frac{\epsilon_{cl}}{\kappa_l - \kappa_{cl}} - \frac{\epsilon_a}{3\kappa_a}\right)\left(\frac{3}{\kappa_l - \kappa_{cl}} - \frac{1}{\kappa_l}\right)^{-1} \tag{10}$$

$$\frac{\kappa_l - \kappa_{cl}}{\kappa_a - \kappa_{cl}}\left(\frac{\kappa_a}{\kappa_l}\right)^{1/3} = 1 - P \tag{11}$$

Numerical calculation with models B and C

To assess the effects of the cell wall conductivity κ_w on dielectric behavior of a cell suspension, numerical calculations were made using model B (Fig. 2). With $\kappa_w/\kappa_a = 1$, there are a main dispersion (β_1-dispersion) around a few MHz and a very small dispersion that appears as a small conductivity change above 100 MHz because this calculation is made under the condition of $\kappa_i > \kappa_a$. When $\kappa_w/\kappa_a < 1$, an additional dispersion (β_2-dispersion) appears between 10 and 100 MHz and its magnitude increases with decreasing the κ_w/κ_a ratio. Further, the β_1-dispersion is also influenced by the κ_w/κ_a ratio; with decreasing the κ_w/κ_a ratio, the characteristic frequency of the β_1-dispersion trends to shift to lower frequencies, the low-frequency limit of the relative permittivity ϵ_l increases and the low-frequency limit of the conductivity κ_l decreases. These numerical results indicate that the cell wall should be incorporated in the theoretical analysis of dielectric behavior of yeast cells.

Next we numerically examined the contribution of the vacuole to dielectric behavior of yeast cells using model C (Fig. 3). The β_2-dispersion due to the vacuole appears in the frequency range of 10 to 100 MHz, where the β_2-dispersion due to the cell wall is also predictable as seen in Fig. 2. The increase in the volume ratio P_v of the vacuole to the protoplasm increases the magnitude of the β_2-dispersion and decreases the characteristic frequency of the β_1-dispersion, although the low-frequency limits of the relative permittivity and conductivity are independent of P_v.

These calculations suggest that both of the cell wall and the vacuole could be a candidate of β_2-dispersion of yeast cells.

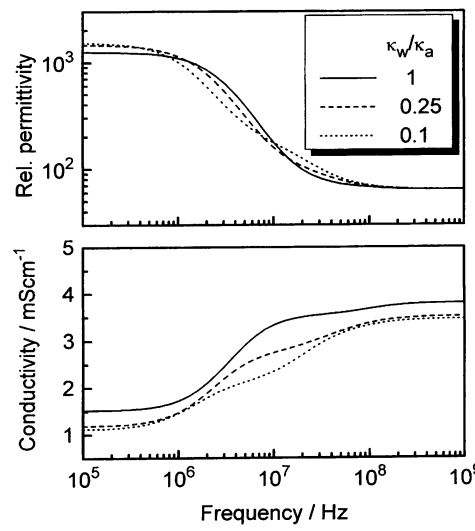

FIGURE 2 Frequency dependence of the relative permittivity and conductivity calculated using model B. In the calculation, the value of the κ_w/κ_a ratio was varied as: 1, 0.25, and 0.1. The parameter values used are as follows: $\epsilon_a = 78$, $\kappa_a = 3$ mS/cm, $\epsilon_w = 60$, $\epsilon_m = 5$, $\kappa_m = 0$ mS/cm, $\epsilon_i = 50$, $\kappa_i = 5$ mS/cm, $R_o = 2.75$ μm, $d_w = 250$ nm, $d_m = 7$ nm, $P = 0.5$.

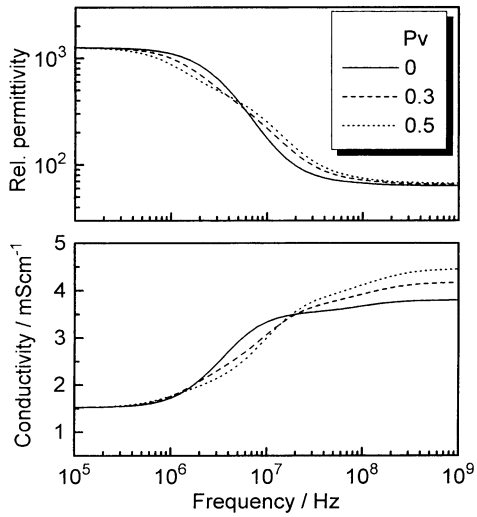

FIGURE 3 Frequency dependence of the relative permittivity and conductivity calculated using model C. In the calculation, the volume ratio P_v of the vacuole to the protoplasm was varied as: 0, 0.3, and 0.5. The parameter values used are as follows: $\epsilon_a = 78$, $\kappa_a = 3$ mS/cm, $\epsilon_w = 60$, $\kappa_w = 3$ mS/cm, $\epsilon_m = 5$, $\kappa_m = 0$ mS/cm, $\epsilon_{cs} = 50$, $\kappa_{cs} = 5$ mS/cm, $\epsilon_t = 5$, $\kappa_t = 0$ mS/cm, $\epsilon_{vi} = 50$, $\kappa_{vi} = 10$ mS/cm, $R_o = 2.75$ μm, $d_w = 250$ nm, $d_m = 7$ nm, $d_t = 7$ nm, $P = 0.5$.

MATERIALS AND METHODS

Preparation of yeast cells

The yeast strains (***Saccharomyces cerevisiae***) used were yw21-1B (wild-type) and yw21-1A (vacuole-deficient mutant), which were a kind gift from Dr. Y. Ohsumi (University of Tokyo). The cells were cultured at 27°C in the YEPD medium containing 1% yeast extract, 2% glucose, and 2% polypeptone. The cells were harvested at the early stationary growth phase after 1-day culture and washed with a 20 mM KCl solution, and finally resuspended in KCl solutions (pH 5.6–6.2) ranging from 10 to 80 mM for dielectric measurements. We did not used buffered KCl solutions because there was no discernible difference in dielectric behavior of yeast cells in the pH range 3–8 when measurements were carried out at least within 1 h.

Dielectric measurements

Relative permittivity and conductivity over a frequency range of 10 kHz to 200 MHz were measured using 4192A and 4191A Impedance Analyzers with a 16092A Spring Clip fixture (Hewlett-Packard Co., Palo Alto, CA). The measurement cells used are similar to those described in previous papers (Asami et al., 1984; Asami and Yamaguchi, 1992). For the raw data measured, correction for residual inductance and stray capacitance arising from the measurement cell and the fixture was made based on a distributed circuit model (Asami et al., 1984).

Microwave dielectric measurements over a frequency range of 200 MHz to 13.5 GHz were carried out using a 8719C Network Analyzer with a 85070A Dielectric Probe Kit (Hewlett-Packard) including an open-ended coaxial probe and a measurement software. All measurements were made at 25°C.

Determination of volume fraction

After dielectric measurements, the volume fraction of the cell suspensions was calculated from the mean cell diameter microscopically determined with interference differential optics and the cell count from a Coulter Multisizer II (Coulter Electronics Ltd., Luton, Beds., England). Because the cells were nearly spherical in the early stationary growth phase, the mean cell volume was calculated from the mean cell diameter by assuming a sphere for the cells.

RESULTS

Dielectric behavior of wild-type yeast and vacuole-deficient mutant in the early stationary growth phase

In the early stationary growth phase, the great majority of the cells did not have buds and were nearly spherical.

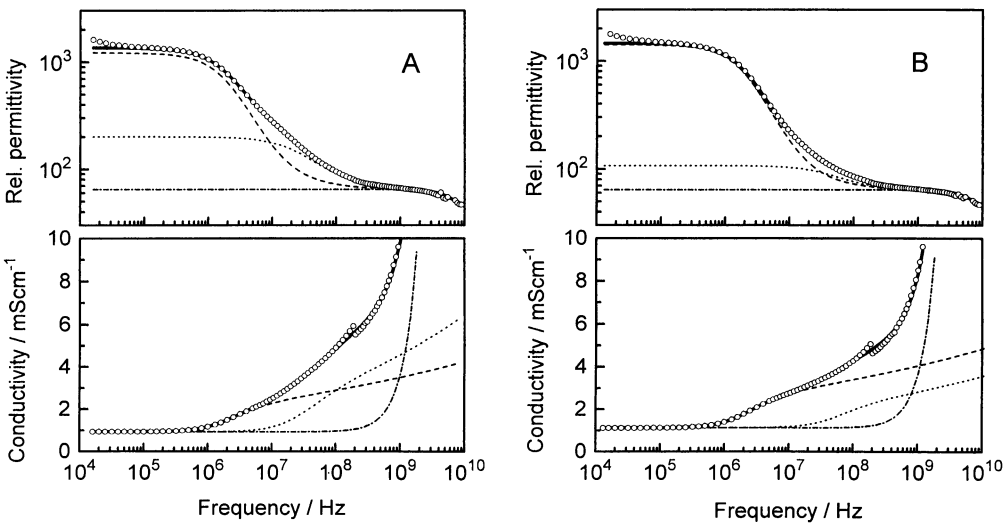

FIGURE 4 Dielectric behavior of suspensions of (*a*) wild-type and (*b*) vacuole-deficient mutant cells in the early stationary growth phase. The cells were suspended in a 20 mM KCl solution. The solid lines are best-fit curves calculated from Eq.12 with parameters shown in Table 1. In the relative permittivity plots, the broken lines, β_1-dispersion + ϵ_h + $\Delta\epsilon_3$; the dotted lines, β_2-dispersion + ϵ_h + $\Delta\epsilon_3$; the dot-dash lines, γ-dispersion + ϵ_h. In the conductivity plots, the broken lines, β_1-dispersion + κ_l; the dotted lines, β_2-dispersion + κ_l; the dot-dash lines, γ-dispersion + κ_l. The increase in relative permittivity at frequencies below 100 kHz is due to an electrode polarization effect.

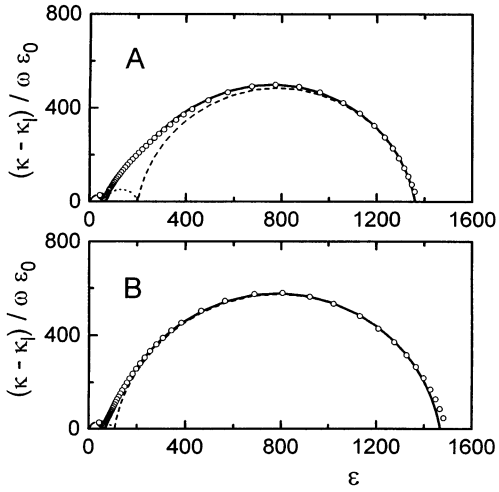

FIGURE 5 Cole-Cole plots of the data shown in Fig. 6 for (*a*) wild-type and (*b*) vacuole-deficient mutant cells. The solid lines were calculated from Eq. 12. The broken and dotted lines indicate the β_1-dispersion and β_2-dispersion, respectively.

Under a phase contrast microscope, a vacuole was clearly observed in the wild-type cells but not in the mutant cells. Fig. 4 shows frequency dependence of the relative permittivity and conductivity of wild-type and vacuole-deficient mutant cells suspended in a 20 mM KCl solution. Both types of cells showed marked dielectric dispersion between 100 kHz and 1 GHz and dielectric dispersion of water above 1 GHz. In the frequency range from 10 MHz to 1 GHz, a small but definitive difference in dielectric behavior was found between the wild-type and the mutant. The Cole-Cole plots of the data <1 GHz were not symmetrical, especially for the wild-type cells (Fig. 5), which could not sufficiently be simulated by a single dispersion term although formalisms applicable to asymmetrical dispersions, such as the Davidson-Cole equation (Davidson and Cole, 1950) and the Havriliak-Negami equation (Havriliak and Negami, 1967), were tested. It is, therefore, reasonable to assume an additional dispersion at the high-frequency side of the main dispersion. Thus, we attempted to describe the observed dispersion curves including the dispersion of water by a sum of three dispersion terms, for which the Cole-Cole formalism (Cole and Cole, 1941) is assumed.

$$\epsilon^* = \epsilon_h + \frac{\Delta\epsilon_1}{1 + (jf/f_{c1})^{1-\alpha_1}} + \frac{\Delta\epsilon_2}{1 + (jf/f_{c2})^{1-\alpha_2}} + \frac{\Delta\epsilon_3}{1 + (jf/f_{c3})^{1-\alpha_3}} + \frac{\kappa_l}{j2\pi f\epsilon_0} \quad (12)$$

where $\Delta\epsilon$ is magnitude of dielectric dispersion, f_c characteristic frequency, α Cole's parameter, κ_l the low-frequency limit of conductivity, and the subscripts 1, 2, and 3 refer to β_1-dispersion (main dispersion), β_2-dispersion (additional dispersion), and γ-dispersion (water dispersion), respectively.

The agreement between the observed dispersion curves and the theoretical ones calculated from Eq. 12 is satisfactory for the range between 100 kHz and 10 GHz. The best-fit parameters of Eq. 12 are listed in Table 1, which also includes the results for the cells suspended in 10, 40, and 80 mM KCl solutions. Significant differences between the wild-type and mutant cells were found in the magnitude $\Delta\epsilon_2$ and characteristic frequency f_{c2} of the β_2-dispersion, indicating a contribution from the vacuole. The β_2-dispersion of the vacuole-deficient mutants was influenced by the external conductivity κ_a; $\Delta\epsilon_2$ decreased and f_{c2} increased with increasing κ_a. This implies that the β_2-dispersion of the mutant cells is related to the cell wall that is in contact with the external medium. However, the β_2-dispersion of the wild-type cells was larger in magnitude and less sensitive to the external conductivity than that of the mutant cells. For the wild-type cells both the vacuole and the cell wall may contribute to the β_2-dispersion.

The γ-dispersion was slightly different from the dispersion of bulk water. The characteristic frequency (f_{c3} = 14 GHz) was shifted by ~25% from that of pure water and the dispersion curve was broader than that of pure water. However, there was no difference in the dielectric parameters of the γ-dispersion between the two types of cells.

TABLE 1 The phenomenological parameters estimated for the dielectric dispersion curves of yeast cells in the early stationary growth phase using Eq. 12 (The data for both wild-type and mutant cells suspended in a 20 mM KCl are the same as in Figs. 4 and 5)

Yeast	KCl mM	κ_l mS/cm	$\Delta\epsilon_1$	f_{c1} MHz	α_1	$\Delta\epsilon_2$	f_{c2} MHz	α_2	$\Delta\epsilon_3$
Wild-type	10	0.53	1090	1.4	0.09	160	26	0.24	59
	20	0.94	1160	2.0	0.11	136	28	0.17	62
	40	1.94	1120	2.6	0.12	128	25	0.14	62
	80	3.95	1050	3.4	0.14	110	23	0.12	61
Mutant	10	0.60	1345	1.5	0.11	54	50	0.14	61
	20	1.13	1360	2.1	0.10	43	50	0.14	61
	40	2.22	1300	2.9	0.08	32	60	0.14	61
	80	4.17	1326	3.8	0.08	18	80	0.14	61

$\epsilon_h = 4, f_{c3} = 14$ GHz, $\alpha_3 = 0.04$

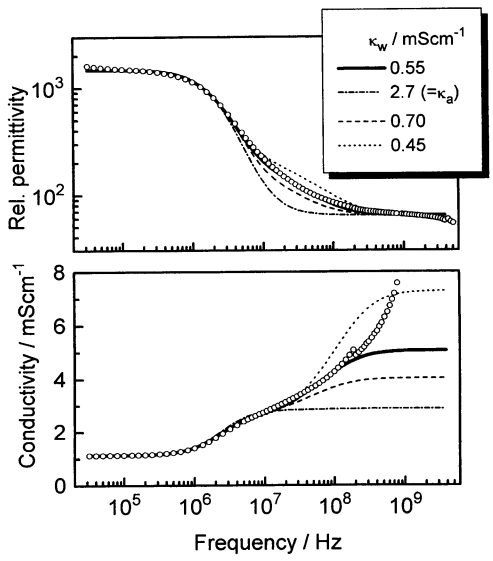

FIGURE 6 Dielectric dispersion of vacuole-deficient mutant cells simulated using model B. The value of κ_w/mScm^{-1} was varied as: 0.55, 2.7, 0.7, and 0.45. The parameter values used are shown in Table 2.

Analysis of vacuole-deficient mutant based on model B

As a first approximation, model B may be applicable to vacuole-deficient mutant cells. Fig. 6 and Table 2 show the curve-fitting procedure based on model B for the dispersion curve shown in Fig. 4 *a*. When $\kappa_w = \kappa_a$, there is considerable discrepancy between the observed and calculated curves in the frequency range from 10 to 100 MHz. The discrepancy is reduced by adjusting κ_w. The best-fit curve was obtained with $\kappa_w = 0.55$ mS/cm and the agreement between the observed and calculated curves is quite satisfactory. The difference in conductivity between the theoretical and experimental curves at frequencies $>10^8$ Hz corresponds mostly to the contribution of water dispersion that is not considered in numerical calculation with the model.

In this analysis we adopted 0.25 μm for the wall thickness d_w because the wall thickness estimated from electron micrographs was between 0.2 and 0.3 μm (Y. Ohsumi, personal communication). The uncertainty in the wall thickness causes some errors in the estimation of the cell parameters, which were assessed as $0.50 < \kappa_w$/mS cm^{-1} < 0.63, $5.2 > \epsilon_m > 5.8$, and $8 < \kappa_i$/mS cm^{-1} < 10 for $0.2 < d_w/\mu m < 0.3$.

Table 3 shows the best-fit parameters estimated for the data of the mutant cells in Table 1. The estimated parameters are independent of the KCl concentration in medium except the κ_w/κ_a ratio. The κ_w/κ_a ratio increases with decreasing KCl concentration, which could result from the Donnan effect because of fixed charges in the wall, as pointed out previously (Asami, 1977b).

Analysis of wild-type yeast based on model C

As seen in the numerical simulations (Figs. 2 and 3), the β_2-dispersions due to the wall and the vacuole appear in a similar frequency range. This makes it difficult to analyze the dielectric behavior of the wild-type cells by the curve-fitting technique with model C. Our strategy for solving this problem is that the wall conductivity and the membrane capacitance are separately determined and then the curve-fitting is made by adjusting the other parameters. The cell wall conductivity can be estimated from the relationship between the κ_i/κ_a ratio and the volume fraction using Eq. 11. In Fig. 7 *a*, the κ_i/κ_a ratio measured for the wild-type cells suspended in a 20 mM KCl solution is plotted against the volume fraction that was estimated as described in Materials and Methods. The κ_w/κ_a ratio was estimated to be 0.24 by fitting Eq. 11 to the data points. The membrane capacitance C_m was also estimated to be 0.65 μF/cm^2 from the plots of the ϵ_i against the volume fraction using Eq. 10. The values of the κ_w/κ_a ratio and C_m are consistent with those estimated for the mutant cells (Table 3).

Using the estimated values of κ_w and C_m as fixed values, the dielectric dispersion curves of the wild-type cells were analyzed by the curve-fitting technique based on model C. Fig. 8 shows the best-fit curve with the value of P_v calculated from the mean diameters of the vacuole and the cell, which were determined with an interference differential microscope. The best-fit parameters are shown in Table 4. Although the estimated values of ϵ_t, κ_{vi}, and κ_{cp} may include some errors because of uncertainty in determination of P_v, it is clear that model C provides in a better simulation for the dielectric behavior of wild-type cells than the model B (that corresponds to the model C with $P_v = 0$). This result may suggest that the β_2-dispersion of wild-type cells is composed of two dispersions arising from the simultaneous presence of cell wall and vacuole.

TABLE 2 The phase parameters of model B used for calculation of the theoretical curves in Fig. 6 (the best-fit curve was obtained with κ_w = 0.55 mS/cm)

κ_w mS/cm	κ_w/κ_a	ϵ_m	ϵ_i	κ_i mS/cm	P
0.55	0.20	5.5	50	9.3	0.49
2.80 (=κ_a)	1	5.5	59	3.1	0.65
0.7	0.25	5.5	51	6.7	0.50
0.45	0.16	5.5	50	15	0.48

$\epsilon_a = 77$, $\kappa_a = 2.80$ mS/cm, $\epsilon_w = 60$, $\kappa_m = 0$ S/cm, $R_o = 2.60$ μm, $d_w = 0.25$ μm, $d_m = 7$ nm.

TABLE 3 The phase parameters of vacuole-deficient mutant cells estimated using model B

KCl mM	κ_w mS/cm	κ_w/κ_a	ϵ_m	κ_i mS/cm
10	0.42	0.29	5.4	8.9
20	0.55	0.20	5.5	9.3
40	0.70	0.13	5.2	9.0
80	1.0	0.10	5.1	9.0

$\epsilon_a = 77$, $\epsilon_w = 60$, $\epsilon_i = 50$, $\kappa_m = 0$ S/cm, $R_o = 2.60$ μm, $d_w = 0.25$ μm, and $d_m = 7$ nm. Mean membrane capacitance was 0.67 μF/cm^2.

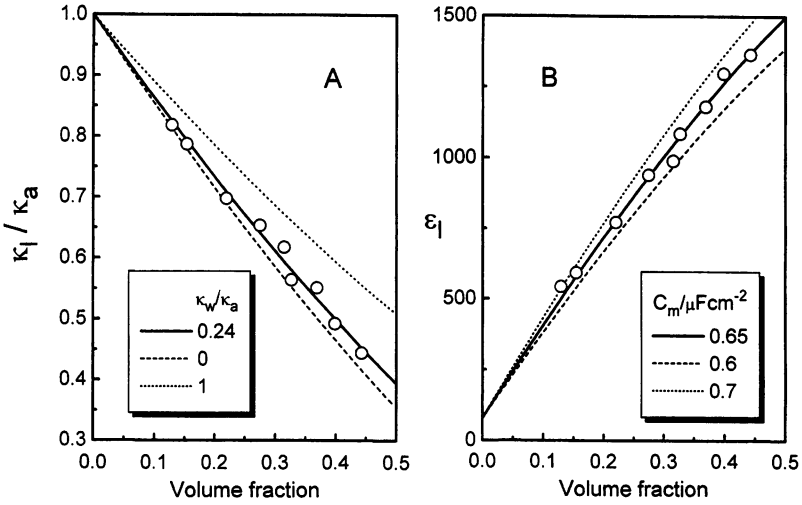

FIGURE 7 Estimation of (*a*) κ_w and (*b*) C_m of wild-type yeast cells from the observed κ_i, ϵ_i and volume fraction. (*a*) The κ_i/κ_a ratio was plotted against the volume fraction. The curves were calculated from Eq. 11 when κ_w/κ_a is 1.0, 0.24 (the best-fit value), and 0. (*b*) The ϵ_i was plotted against the volume fraction. The curves were calculated from Eq. 10 with C_m of 0.70, 0.65 (the best-fit value) and 0.60 μF/cm^2. The other parameter values used are: d_w = 0.25 μm, R_o = 2.75 μm, and κ_w/κ_a = 0.24.

DISCUSSION

We have found that yeast cells in the stationary growth phase have an additional dispersion (β_2-dispersion) between the main dispersion (β_1-dispersion) and the γ-dispersion (water dispersion). The β_2-dispersion has never been observed for yeast cells in the logarithmic growth phase, because the broadening of the β_1-dispersion makes it difficult to distinguish the β_2-dispersion from the β_1-dispersion (Asami et al., 1976). The broadening that results from a distribution of relaxation times could not be interpreted simply in terms of the distribution of cell sizes and cytoplasmic conductivities (Markx et al., 1991); thus, for the full interpretation, other factors are required, such as the variation of cell shapes because there are many budding cells in various cell-division states in the logarithmic growth phase.

The β_2-dispersion for the vacuole-deficient mutant cells has been successfully interpreted in terms of interfacial polarization due to the cell wall. However, the vacuole is the major contribution to the β_2-dispersion for the wild-type cells, although the cell wall also contribute to it. Although dielectric dispersions due to bound water and biological materials such as amino acids, proteins, and nucleic acids are expected in a frequency range of 1 MHz to several hundred MHz (e.g., Grant et al., 1978; Pethig, 1979; Takashima, 1989), we believe that their contributions to the β_2-dispersion is very small because there is no discernible β_2-dispersion for spherical erythrocytes that contain no intracellular structure but hemoglobin at a high concentration (Asami et al., 1989).

With a 20 mM KCl solution for the medium, the conductivity ratio of the cell wall to the medium, κ_w/κ_a, was 0.20 for the mutant cells, as estimated by fitting model B to the observed dispersion data, and 0.24 for the wild-type cells, when determined from the relationship between the κ_i/κ_a ratio and the volume fraction. Our result is not consistent with our previous conclusion that the wall conductivity is almost the same as that of the external media (Asami et al., 1976; Asami, 1977b). Our previous conclusion should be amended because it was drawn from inappropriate analyses in which concentrated yeast suspensions including (non-spherical) budding cells were dealt with using Pauly-Schwan's equation that holds for only dilute suspensions of spherical cells.

The κ_w/κ_a ratio depended on the medium conductivity, which may be explained by the Donnan effect due to fixed charges in the cell wall, as first pointed out by Carstensen et

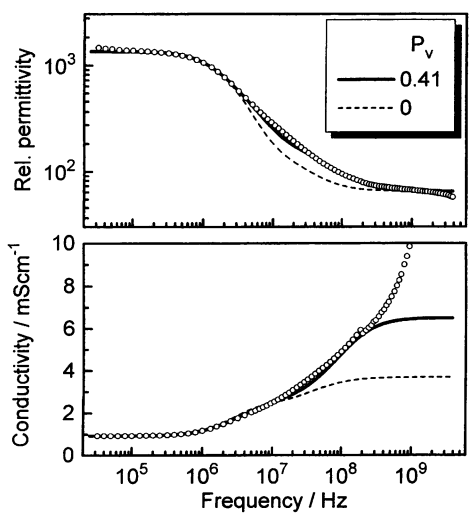

FIGURE 8 Dielectric dispersion of wild-type cells simulated using model C. The value of P_v used are: 0.41 (the best-fit value) and 0. The parameter values used are shown in Table 4.

TABLE 4 The phase parameters of wild-type cells estimated using models B and C

Model	ϵ_m	ϵ_{cs}	κ_{cs} mS/cm	ϵ_t	κ_{vi} mS/cm	P
C	5.2	50	12	12	15	0.56
B	5.2	58	6			0.56

ϵ_a = 77, κ_a = 2.80 mS/cm, ϵ_w = 60, κ_w = 0.67 mS/cm, κ_m = 0 S/cm, κ_t = 0 S/cm, ϵ_{vi} = 70, R_o = 2.35 μm, R_v = 1.56 μm, d_w = 0.25 μm, d_m = 7 nm, d_t = 7 nm, C_m = 0.65 μF/cm^2 and $C_t = \epsilon_t\epsilon_o/d_t$ = 1.5 μF/cm^2.

al. (1965). With an increase in the KCl concentration of the medium, the κ_w/κ_a ratio tends to reach a constant value of ~0.1, which may be regarded as the porosity of the cell wall.

The membrane capacitance C_m of the yeast plasma membranes was estimated to be 0.65 μF/cm^2 using Hanai's mixture equation and model B or C including the wall. The value would be a better estimate than the value of 1 μF/cm^2 obtained in our previous study (Asami et al., 1976) using Wagner's mixture equation and model A. The present value is close to the values for the membranes with smooth surfaces, such as the plasma membranes of erythrocytes and plant protoplasts (Asami et al., 1989, 1992) and solvent-free bilayer lipid membranes (White, 1986). Usually, the specific membrane capacitance may be between 0.6 and 0.9 μF/cm^2, and infoldings and microvillation of the plasma membrane increase the apparent membrane capacitance (Irimajiri et al., 1987). Our results, therefore, indicates low degree of infolding or invagination in the yeast plasma membranes.

We would like to thank Dr. T. Hanai and Dr. A. Irimajiri for critical readings of this manuscript.

REFERENCES

Asami, K. 1977a. Dielectric behavior of yeast cell suspensions: Effect of some chemical agents and physical treatments on the plasma membrane and the cytoplasm. *Bull. Inst. Chem. Res. Kyoto Univ.* 55:283–309.

Asami, K. 1977b. Dielectric properties of protoplasm, plasma membrane and cell wall in yeast cells. *Bull. Inst. Chem. Res. Kyoto Univ.* 55: 394–414.

Asami, K., T. Hanai, and N. Koizumi. 1976. Dielectric properties of yeast cells. *J. Membrane Biol.* 28:169–180.

Asami, K., T. Hanai, and N. Koizumi. 1977. Dielectric properties of yeast cells: effect of some ionic detergents on the plasma membrane. *J. Membrane Biol.* 34:145–156.

Asami, K., A. Irimajiri, T. Hanai, N. Shiraishi, and K. Utsumi. 1984. Dielectric analysis of mitochondria isolated from rat liver. I. Swollen mitoplasts as simulated by a single-shell model. *Biochim. Biophys. Acta.* 788:559–569.

Asami, K., Y. Takahashi, and S. Takashima. 1989. Dielectric properties of mouse lymphocytes and erythrocytes. *Biochim. Biophys. Acta.* 1010: 49–55.

Asami, K., and T. Yamaguchi. 1992. Dielectric spectroscopy of plant protoplasts. *Biophys. J.* 63:1493–1499.

Bruggeman, D. A. G. 1935. Berechnug vershiedener physikalischen Konstanten von heterogenen Substanzen. *Ann. Phys. Lpz.* 24:636–664

Carstensen, E. L., H. A. Cox, Jr., W. B. Mercer, and L. A. Natale. 1965. Passive electrical properties of microorganisms. I. Conductivity of *Escherichia coli* and *Micrococcus lysodeikticus*. *Biophys. J.* 5:289–300.

Clausse, M. 1983. Dielectric properties of emulsions and related systems. *In* Encyclopedia of Emulsion Technology, Vol. 1. P. Becher, editor. Marcel Dekker Inc., New York. 481–715.

Cole, K. S. 1968. Membranes, Ions and Impulses. University of California Press, Berkeley.

Cole, K. S., and R. H. Cole. 1941. Dispersion and absorption in dielectrics. I. Alternating current characteristics. *J. Chem. Phys.* 9:341–351.

Davey, C. L., H. M. Davey, and D. B. Kell. 1992. On the dielectric properties of cell suspensions at high volume fractions. *Bioelectrochem. Bioenerg.* 28:319–340.

Davidson, D. W., and R. H. Cole. 1950. Dielectric relaxation in glycerin. *J. Chem. Phys.* 18:1417.

Foster, K. R., and H. P. Schwan. 1989. Dielectric properties of tissues and biological materials: a critical review. *Crit. Rev. Biomed. Engin.* 17: 25–104.

Furhr, G., J. Gimsa, and R. Glaser. 1985. Interpretation of electrorotation of protoplasts. I. Theoretical considerations. *Studia Biophys.* 108: 149–164.

Gimsa, J., G. Furhr, and R. Glaser. 1985. Interpretation of electrorotation of protoplasts. II. Interpretation of experiments. *Studia Biophys.* 109: 5–14.

Gimsa J., P. Marszalek, U. Loewe, and T. Y. Tsong. 1991. Dielectrophoresis and electrorotation of neurospora slime and murine myeloma cells. *Biophys. J.* 60:749–760.

Grant, E. H., R. J. Sheppard, and G. P. South. 1978. Dielectric Behaviour of Biological Molecules in Solution. Oxford University Press, Oxford.

Hanai, T. 1960. Theory of the dielectric dispersion due to the interfacial polarization and its application to emulsion. *Kolloid Z.* 171:23–31.

Hanai, T. 1968. Electrical properties of emulsions. *In* Emulsion Science. P. Sherman, editor. Academic Press, New York. 353–478.

Hanai, T., K. Asami, and N. Koizumi. 1979. Dielectric theory of concentrated suspension of shell-spheres in particular reference to the analysis of biological cell suspensions. *Bull. Inst. Chem. Res. Kyoto Univ.* 57: 297–305.

Hanai, T., T. Imakita, and N. Koizumi. 1982. Analysis of dielectric relaxation of w/o emulsions in the light of theories of interfacial polarization. *Colloid Polymer Sci.* 260:1029–1034.

Harris, C. M., and D. B. Kell. 1983. The radio-frequency dielectric properties of yeast cells measured with a rapid, automated frequency-domain dielectric spectrometer. *Bioelectrochem. Bioenerg.* 11:15–28.

Havriliak, S., and S. Negami. 1967. A complex plane representation of dielectric and mechanical relaxation processes in some polymers. *Polymer.* 8:161–210.

Irimajiri, A., K. Asami, T. Ichinowatari, and Y. Kinoshita. 1987. Passive electrical properties of the membrane and cytoplasm of cultured rat basophil leukemia cells. II. Effects of osmotic perturbation. *Biochim. Biophys. Acta.* 896:214–223.

Irimajiri, A., Y. Doida, T. Hanai, and A. Inouye. 1978. Passive electrical properties of cultured murine lymphoblast (L5178Y) with reference to its cytoplasmic membrane, nuclear envelope, and intracellular phases. *J. Membr. Biol.* 38:209–232.

Irimajiri, A., T. Hanai, and A. Inouye. 1975. Evaluation of a conductometric method to determined the volume fraction of the suspensions of biomembrane-bounded particles. *Experientia.* 31:1373–1374.

Irimajiri, A., T. Hanai, and A. Inouye. 1979. A dielectric theory of "multi-stratified shell" model with its application to a lymphoma cell. *J. Theor. Biol.* 78:251–269.

Ishikawa, A., T. Hanai, N. Koizumi. 1981. Evaluation of relative permittivity and electrical conductivity of ion-exchange beads by analysis of high-frequency dielectric relaxations. *Jpn. J. Appl. Phys.* 20:79–86.

Kaneko, H., K. Asami, and T. Hanai. 1991. Dielectric analysis of sheep erythrocyte ghost. Examination of applicability of dielectric mixture equations. *Colloid Polymer Sci.* 269:1039–1044.

Markx, G. H., C. L. Davey, and D. B. Kell. 1991. To what extent is the magnitude of the Cole-Cole α of the β-dielectric dispersion of cell suspensions explicable in terms of the cell size distribution? *Bioelectrochem. Bioenerg.* 25:195–221.

Maxwell, J. C. 1873. Treatise on Electricity and Magnetism. Oxford University Press, London.

Pauly, H., and H. P. Schwan. 1959. Uber die Impedanz einer Suspension von kugelformigen Teilchen mit einer Schale. *Z. Naturforsch.* 14b: 125–131.

Pethig, R. 1979. Dielectric and Electronic Properties of Biological Materials. John Wiley & Sons, New York.

Schwan, H. P. 1957. Electrical properties of tissue and cell suspensions. *In* Advances in Biological and Medical Physics, Vol. 5. J. H. Lawrence and C. A. Tobias, editors. Academic Press, New York. 147–209.

Schwan, H. P. 1987. Biological effects of non-ionizing radiations: Cellular properties and interactions. The Lauriston S. Taylor Lectures, No. 10. National Council on Radiation Protection and Measurements.

Sugiura, Y., and S. Koga. 1965. Dielectric behavior of yeast cells treated with $HgCl_2$ and cetyl trimethyl ammonium bromide. *Biophys. J.* 5:439–445.

Sugiura, Y., S. Koga, and H. Akabori. 1964. Dielectric behavior of yeast cells in suspension. *J. Gen. Appl. Microbiol.* 10:163–174.

Takashima, S. 1989. Electrical Properties of Biopolymers and Membranes. Adam Hilger, Bristol, England.

Wagner, K. W. 1914. Erklarung der dielectrishen Nachwirkungs vorgange auf Grund Maxwellscher Vorstellungen. *Arch. Electrotechnik.* 2:371–387.

White, S. H. 1986. The physical nature of planar bilayer membranes. *In* Ion channel reconstitution. C. Miller, editor. Plenum Press, New York. 2–35.

Zhang, H. Z, K. Sekine, T. Hanai, and N. Koizumi. 1983. Dielectric observations of polystyrene microcapsules and the theoretical analysis with reference to interfacial polarization. *Colloid Polymer Sci.* 261: 381–389.